

# The planet search program at the ESO Coudé Echelle spectrometer<sup>\*</sup>

## I. Data modeling technique and radial velocity precision tests

M. Endl<sup>1,2</sup>, M. Kürster<sup>1</sup>, and S. Els<sup>1,3</sup>

<sup>1</sup> European Southern Observatory, Casilla 19001, Vitacura, Santiago 19, Chile

<sup>2</sup> Universität Wien, Institut für Astronomie, Türkenschanzstrasse 17, 1180 Wien, Austria

<sup>3</sup> Universität Heidelberg, Institut für Theoretische Astrophysik, Tiergartenstrasse 15, 69121 Heidelberg, Germany

Received 27 January 2000 / Accepted 24 July 2000

**Abstract.** We present the modeling technique we apply to analyse data of the ESO Coudé Echelle Spectrometer (CES) planet search program, in order to obtain high precision stellar radial velocity (RV) measurements. The detection of the Doppler reflex motion of a star due to an orbiting planet has so far been the most successful method to discover planetary companions to solar-type stars. The first extrasolar planet discovered by the CES program is the companion to the young (ZAMS) G0V star  $\iota$  Hor (Kürster et al. 2000). To achieve a high long-term RV measurement stability the CES spectra are self-calibrated by a superimposed iodine vapor ( $I_2$ ) reference spectrum. In the modeling process a multi-parameter  $\chi^2$ -optimization is employed to generate an accurate description of the observation. We largely follow the general modeling approach for  $I_2$ -calibrated data outlined by Butler et al. (1996) and Valenti et al. (1995). The sharp  $I_2$  reference lines allow the reconstruction of the spectrograph instrumental profile (IP) and the precise determination of the Doppler shift of the stellar absorption lines. We show examples of the application of the modeling technique to CES data obtained over a time span of five and a half years at ESO La Silla. The small spectral bandwidth of only 4.85 nm for CES spectra makes this data challenging for high precision radial velocities. We demonstrate for the known RV-constant star  $\tau$  Cet, for two stars with known extrasolar planets, 51 Peg and 70 Vir, and for  $\alpha$  Men and GJ 570A, two stars from our survey that the achievable RV precision for CES data is 8–15  $\text{ms}^{-1}$ .

**Key words:** methods: data analysis – techniques: radial velocities – stars: planetary systems

### 1. Introduction

Several candidates of extrasolar planets orbiting late-type stars have been found by precision Doppler surveys in the past five years (e.g.: Mayor & Queloz 1995; Marcy & Butler 1996; Cochran et al. 1997; Noyes et al. 1997; Fischer et al. 1999;

Kürster et al. 2000). The aim of these Doppler surveys is the detection of the reflex motion of a star due to the gravitational pull of an unseen planetary companion. This reflex motion causes a small Doppler shift of the stellar spectral lines and hence appears as periodic change in the stellar radial velocity (RV). Since these variations in radial velocity are very small (Jupiter induces a velocity variation of 12.4  $\text{ms}^{-1}$  on the Sun over its orbital period) it is necessary to minimize instrumental measurement errors.

In most precision Doppler surveys a temperature-stabilized iodine vapor ( $I_2$ ) absorption cell has been used as the wavelength reference. During observations the  $I_2$ -cell is located in the light path of the spectrograph and superimposes a dense reference spectrum onto the stellar spectrum. Consequently, all instrumental effects which modulate the stellar spectrum affect the reference spectrum in the same way. To take full advantage of this kind of self-calibration, a sophisticated data modeling technique is mandatory. This includes the reconstruction of the shape of the spectrograph instrumental profile (IP, the instrumental point spread function in dispersion direction) since IP asymmetries cause shifts of the spectral lines and, if not taken into account, lead to an erroneous radial velocity result. Since no standard analysis method can be used for this purpose a special modeling technique has to be applied. We followed and extended the general modeling process for  $I_2$ -calibrated data which was first outlined by Butler et al. (1996) and the spectrograph IP reconstruction by Valenti et al. (1995).

In this article we describe the modeling technique we use to analyse the data collected by the southern hemisphere planet search program carried out at the 1.4m CAT telescope and the Coudé Echelle Spectrometer (CES) at ESO La Silla (Kürster et al. 1994; Hatzes et al. 1996). The CES planet search program has been observing a sample of 40 solar-type stars since Nov. 1992. The RV-precision for CES data is mostly limited by the very small spectral bandwidth of only 4.85 nm. However, we are able to verify an achievable RV precision of 8–15  $\text{ms}^{-1}$  by using the RV-constant stars  $\tau$  Cet,  $\alpha$  Men, GJ 570A, and two stars with known extrasolar planets, 51 Peg and 70 Vir, as a test ground. The CES instrument was upgraded in April 1998 by installing the new Very Long Camera yielding a higher resolving power ( $R = 230,000$ ) and an even smaller spectral coverage

---

Send offprint requests to: M. Endl (endl@astro.univie.ac.at)

<sup>\*</sup> Based on observations collected at the European Southern Observatory, La Silla

(depending on which CCD is used). Results presented in this article all refer to the CES configuration (with the Long Camera,  $R = 100,000$ ) prior to this modification. Although the main goal of this work was to optimize the RV measurement precision of the CES, we emphasize improved IP reconstruction techniques and the flexibility to use this method with any spectrograph, calibrated by an  $I_2$ -cell.

The modeling can be divided into the following three major steps:

**Step 1:** Reconstruction of instrumental effects and spectrograph instrumental profiles by modeling pure iodine spectra using a high resolution Fourier Transform Spectrum (FTS) of the  $I_2$ -cell.

**Step 2:** Deconvolution of ‘template’ stellar spectra using the Maximum Entropy Method (MEM) and the instrumental profiles obtained by step 1.

**Step 3:** Complete modeling of the combined iodine and stellar spectrum. The iodine FTS and the deconvolved stellar spectrum from step 2 serve as model templates to synthesize the observation. The Doppler shift between the iodine reference and the stellar absorption lines is determined with high accuracy.

In this article we first describe the individual modeling steps, their application to CES data, and present RV-precision test results for  $\tau$  Cet, 51 Peg, 70 Vir and show the long-term RV results for two stars of our sample,  $\alpha$  Men and GJ 570A, which verify the long-term precision we found for  $\tau$  Cet. The discovery of the extrasolar planet around  $\iota$  Hor by this analysis method has already been reported elsewhere (Kürster et al. 2000). A full analysis of the complete CES planet search data will be presented in a forthcoming paper (Endl et al., in prep.).

## 2. The CES instrument and the iodine cell

The Coudé Echelle Spectrometer (CES) at the ESO La Silla observatory is a conventional non-stabilized spectrograph offered to the whole astronomical community and for use in all kinds of high resolution spectroscopic observations. The setup of the instrument is changed frequently and reset before each observing run. Thus changes in the behavior of the spectrograph and most of all variations of the instrumental profile are clearly to be expected. All spectra included in this article were taken with the 1.4m CAT telescope, which fed the spectrograph with a direct beam from the telescope. The incoming light is reflected at the telescope from a third mirror into a tube which leads into the Coudé room, where the CES is located. After passing through the entrance slit and a pre-dispersing prism, the light is dispersed at the Echelle grating of the CES. The Camera optics image a small part of one spectral order onto the CCD detector. The CES is not stabilized in any way and the instrument setup (focus, alignment, CCD orientation) is redone frequently; this can lead to significant variations of the IP between individual nights. On smaller timescales the IP is also affected by seeing conditions and the guiding performance of the telescope. The CES  $I_2$ -cell (see also Kürster et al. 1994) is temperature-stabilized at  $50^\circ$  C and located directly in front of the entrance slit of the spectrograph. It is mounted on a short rail in order to move it

easily in and out of the light path. All spectra of the CES planet search program prior to April 1998 (i.e. before the Long Camera at the CES was replaced by the new Very Long Camera) were taken at a central wavelength of 538.9 nm and with the Long Camera yielding a resolving power of  $R = 100,000$  and a spectral range of 4.85 nm. This spectral region is also free of telluric lines, which was confirmed by observing rapidly rotating B-stars. The great advantage of the  $I_2$  self-calibration technique is the fact that all instrumental effects, like wavelength zero-point drifts, changes in the dispersion or resolving power and variations of the instrumental profile are recorded in the numerous  $I_2$  lines. Therefore an appropriate modeling of the iodine spectrum should be able to exploit this information contained in the shape and position of the  $I_2$  lines. One has to bear in mind that the goal is to measure radial velocities with a precision corresponding to a very small fraction of a CCD pixel. For the CES data one pixel represents a velocity span of  $1300 \text{ ms}^{-1}$  while the typical FWHM of the IP is about  $3000 \text{ ms}^{-1}$  wide. It is clear that any asymmetry of the IP has an impact on the velocity information one can retrieve from the data. For a long-term project like the CES planet search it is mandatory to deal with these instrumental effects in order to attain a very high long-term stability for measuring stellar radial velocities. The use of the  $I_2$ -cell for self-calibration and the application of our data modeling technique make it possible to reach this objective. We will now turn to the description of the data modeling.

## 3. The data modeling technique

### 3.1. Step 1: modeling the pure iodine spectrum

The spectrum of molecular iodine vapor ( $I_2$ ) is a dense forest of sharp absorption lines (see Fig. 1). Pure  $I_2$ -spectra are taken either by using a flatfield (white) lamp or by observing a rapidly rotating B-star (which has no apparent spectral features) through the cell.

In general a spectroscopic observation can be mathematically described as (from Valenti et al. 1995):

$$g(x) = \int_{-\infty}^{\infty} f(x') \phi(x - x') dx, \quad (1)$$

where  $g(x)$  is the observed spectrum at a certain position  $x$  on the detector,  $f(x')$  the intrinsic ‘‘source’’ spectrum (i.e. the spectrum before entering the instrument) and  $\phi(x - x')$  the ‘‘convolving’’ function of the corresponding part ( $x - x'$ ) of  $f$ , i.e. the instrumental profile (with the integral over  $\phi(x - x')$  being unity). The discrete version of Eq. (1) is:

$$g(i) = \sum_{j=i-p}^{i+p} f_j \phi_{i-j}. \quad (2)$$

Here the index  $i$  denotes the pixel number of the observation, while  $j$  is the index of the intrinsic spectrum  $f$ .  $p$  is the cut-off of  $\phi$  with  $\phi_{i-j} = 0$  for  $|i - j| > p$ , which constrains the treatment of the indefinitely wide IP only in a reasonably broad region around its maximum (for instance  $p$  can be set to the point where the IP drops below 1% of its maximum value). An

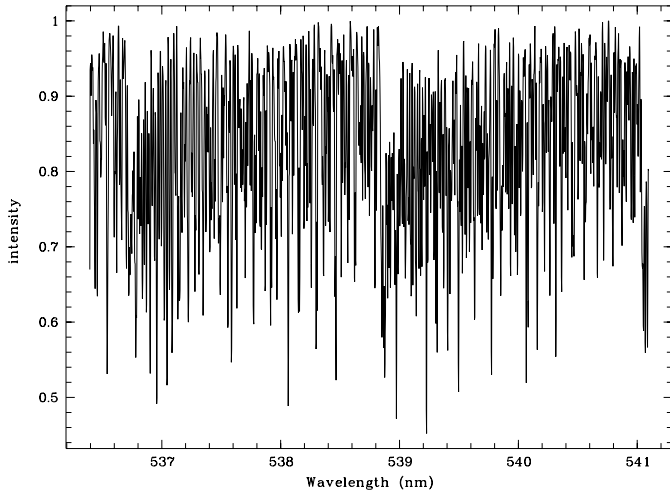


**Fig. 1.** An iodine vapor ( $I_2$ ) absorption spectrum taken with the CES spectrograph on La Silla. The central wavelength is located at 538.9 nm and the spectral coverage is 4.85 nm with a resolving power of 100,000. The light of a flatfield (white) lamp was sent through the  $I_2$ -cell to obtain the absorption spectrum.

ideal instrument would – of course – image the “source” spectrum  $f$  exactly as it is, but diffraction and optical imperfections cause a “smearing” of  $f$  on the detector. This process can be described as a convolution of  $f$  with  $\phi$ . Starting with  $g(i)$  we face an inverse ill-posed problem where a unique solution for  $\phi$  cannot be found. However, an approximation of  $\phi$  can be reconstructed by describing the observation with an appropriate model, including the functional form of  $\phi$  as one or several free model parameters. For a better treatment of the shape of  $\phi$  the model is set up on a sub-pixel grid (usually CCD pixel size and resolving power do not allow a detailed sampling of the IP). With such oversampling Eq. (2) transforms into:

$$g(i) = \sum_{j=q^i}^{q(i+1)-1} \left( \sum_{j'=j-p}^{j+p} f_{j'} \phi_{j-j'} \right) \quad (3)$$

with  $q$  as oversampling factor ( $q = j/i$ ) and  $j$  and  $j'$  as indices on the oversampled grid. All the results presented in this paper were obtained using an oversampling factor of 5.

As the “source” spectrum  $f$  (in Eqs. (1) - (3)) of the iodine we take a high resolution Fourier Transform Spectrum (FTS) which was obtained by scanning our  $I_2$ -cell with the McMath FTS at Kitt Peak, yielding a resolving power of  $R = 400,000$  (determined from the FWHM of the sinc IP of the McMath FTS). To facilitate interpolation within the FTS spectrum we use a spline-interpolated 10 times oversampled version of the FTS. By doing this, strong cutting of line-peaks during the modeling process is avoided, and plain linear interpolation can then be used to read out the spline-interpolated FTS.

Since the IP varies along the spectrum we subdivide it into smaller spectral chunks and model each of these chunks independently (the size of the chunks can be varied; for CES data we typically use spectral chunks of 90 pixels which corresponds to 0.21 nm). In general the modeling process is a multi-parameter

**Table 1.** The free parameters of the model (quantity 2 means that there is one parameter for the iodine and one for the stellar model). Note that not all the IP parameters are used at the same time, their usage depends on the chosen IP reconstruction mode (see text for details).

Quantity	Description
2	Wavelength zero-point
1	Linear dispersion coefficient
2	Linear continuum slope
2	Spectral line depth
2	Normalization
1	2nd-order dispersion coefficient
1	Width of main Gaussian (IP)
1	Width of Box (IP)
1	Width of Lorentz (IP)
4	Amplitudes of satellite Gaussians (IP)

$\chi^2$ -optimization algorithm. Table (1) summarizes and describes all the free parameters of the model. During one modeling iteration each one of the model parameters is optimized by Brent’s method, a parabolic  $\chi^2$ -function interpolation (e.g. Press et al. 1992, Sect. 10.2). The resulting model delivers information on the IP shape, dispersion solution, continuum tilt, and line-depth for each spectral chunk. A second-order dispersion parameter is incorporated because a linear model does not describe chunks of respective size with the necessary accuracy. The line-depth parameter compensates for possible straylight effects, while the slope parameter is used to fit a linear slope to the continuum, if necessary (which for CES spectra is quite often the case). At the beginning of the modeling of one spectral chunk the corresponding part of the  $I_2$ -FTS is read into memory and a “first-guess” model is constructed by parametrizing the  $I_2$ -FTS with starting values and convolving it with a default IP (a simple Gaussian shaped function). Starting values for the parameters are either 0 (for the wavelength zero-point, line-depth and slope parameter) or calculated values, as in the case of the two dispersion parameters, where a global second-order dispersion solution obtained by measuring positions of ThAr-lines delivers these starting values. After this “first-guess” the parameter optimizing algorithm starts and iterates until either  $\chi^2 = N$  (with  $N$  the total number of data points within the chunk) or a satisfactory stop-criterion (like a flat gradient of the  $\chi^2$ -function) is reached. Fig. 2 shows the resulting model along with the observational data for one chunk of a CES iodine spectrum with a high  $S/N$ -ratio.

We have included several different modes to model the IP: in the most simple mode the IP is a single Gaussian, where the width of the Gaussian is the free parameter; in another mode the IP can be simulated by the convolution of a box-function with a Gaussian (Box  $\otimes$  Gaussian). Here two IP parameters are optimized, the width of the box and of the Gaussian. The IP can also be simulated by using a Lorentzian function, for instruments with very extended IP wings. To account for asymmetries the IP can be reconstructed by using a symmetric main Gaussian and up to four smaller Gaussians located in the wings of the IP which are combined into one asymmetric IP (see also Valenti et al. 1995). The width of the main Gaussian and the am-

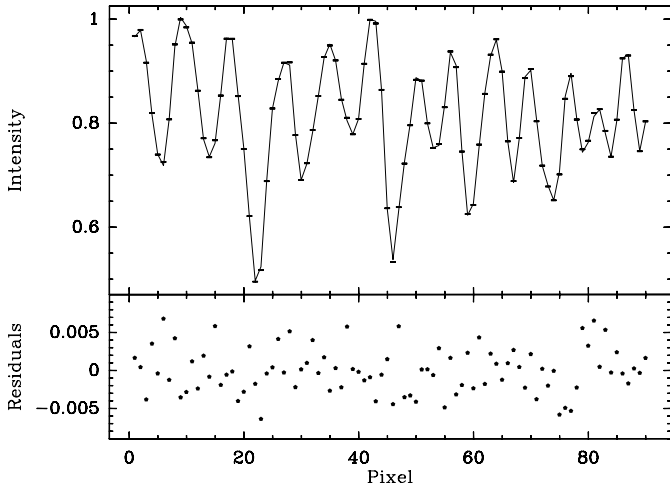


**Fig. 2.** One spectral chunk of a CES  $I_2$ -spectrum (dots and errorbars), containing 90 pixels and spanning from 536.8 nm to 537.0 nm with a mean  $S/N$ -ratio of 1050 (actually the errorbars are so small that they only show up as horizontal bars). The solid line represents the best-fit model based on the  $I_2$ -FTS for this chunk (upper panel), while the lower panel shows the residuals.

plitudes of the satellite Gaussians are the free parameters in this IP modeling mode. The smaller Gaussians located in the wings are added to or subtracted from (when the amplitude becomes negative) the main Gaussian and thus creating an asymmetric shape of the IP. If subtraction from the main Gaussian occurs the modeling prevents negative values for the IP to keep the IP shape physically reasonable. After combining all functions the IP is renormalized to unit area. The positions and widths of the satellite Gaussians are held fixed during the modeling process but both can be selected from an input file, which makes it easier to adapt the technique to different spectrographs.

Furthermore, additional corrections to the IP using the Maximum Entropy Method (MEM) can be applied. MEM is a well known deconvolution method which tends to introduce as little structure as possible in the solution in order to describe the data. For our modeling technique we employ the MEM algorithm described in Kivinen & Warmuth 1997. We exploit the high flexibility of MEM to account for additional IP asymmetries which could only be covered by parametrized functions of high complexity. For this purpose Eq. (3) is rewritten as:

$$g(i) = \sum_{j'=-p}^{-p} \left( \sum_{j=qi-j'}^{q(i+1)-1-j'} f_j \right) \phi_{j'} \quad (4)$$

which gives a matrix equation of the type:

$$\vec{g} = \mathbf{F} \vec{\phi} \quad (5)$$

MEM can now be used to solve Eq. (5) for  $\vec{\phi}$ . The best results are obtained by incorporating the solution already found by optimizing parametrized IP-functions into Eq. (5) in the following way:

$$\vec{g} = \mathbf{F} \mathbf{\Delta} \vec{\phi}_c. \quad (6)$$

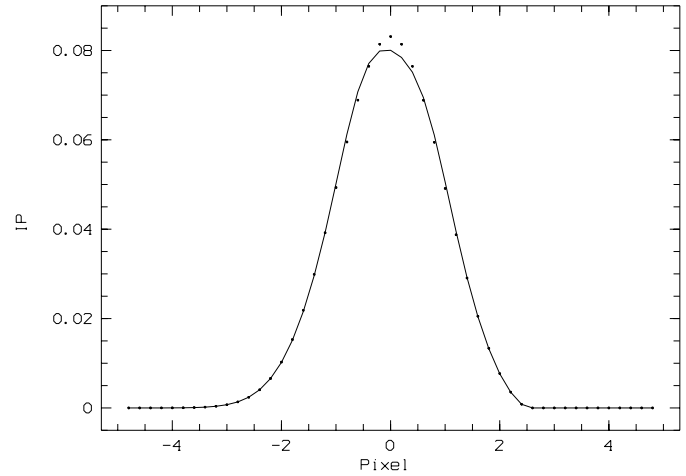


**Fig. 3.** Example for the Maximum Entropy Method correction to the instrumental profile. First the best parametrized function (a Multi-Gaussian) is computed (dots) and then MEM applies additional corrections to determine an improved IP-shape (solid line).

Where  $\mathbf{\Delta}$  is a diagonal matrix containing the elements of  $\vec{\phi}$  found by the (previously described) parametrized IP reconstruction modes. Now this new matrix ( $\mathbf{F} * \mathbf{\Delta}$ ) serves as input for MEM. The solution found by MEM ( $\vec{\phi}_c$ ) represents a correction vector to  $\vec{\phi}$ . An example for the MEM correction to the IP can be seen in Fig. 3.

For CES flatfield  $I_2$ -spectra the best modeling results (with the lowest  $\chi^2$  values) are achieved by using either the Box  $\otimes$  Gaussian or Multi-Gaussian mode along with the MEM correction to reconstruct the instrumental profile. The single Gaussian mode which cannot treat IP asymmetries leads to higher  $\chi^2$  values and the Lorentzian mode was found to be the least adequate IP reconstruction mode. By comparing IPs reconstructed from domeflatfields taken at the beginning and the end of one night we get an estimate of the IP variation on short time scales (see Fig. 4). On larger time scales the frequent setup changes of the instrument can lead to huge differences in the IP form of individual nights. Fig. 5 shows an extreme example of IP variation for two different nights in 1994 and 1995. This example demonstrates clearly that IP modeling is essential for CES data in order to analyse spectra taken over a long time period, covering many different observing runs.

### 3.2. Step 2: deconvolution of the stellar spectrum

In order to establish a complete model of stellar observations through the  $I_2$ -cell, a high resolution “source” spectrum  $f$  (in Eqs. (1) - (4)) for the star is needed. We obtain  $f$  by deconvolving a pure star spectrum (taken without the  $I_2$ -cell) with the IPs reconstructed by step 1. We employ the Maximum Entropy Method (MEM) for the deconvolution process. For this purpose Eq. (4) is reformulated:

$$g(i) = \sum_{j=qi-p}^{q(i+1)+p-1} \left( \sum_{j'=qi-j}^{q(i+1)-j-1} \phi_{j'} \right) f_j \quad (7)$$

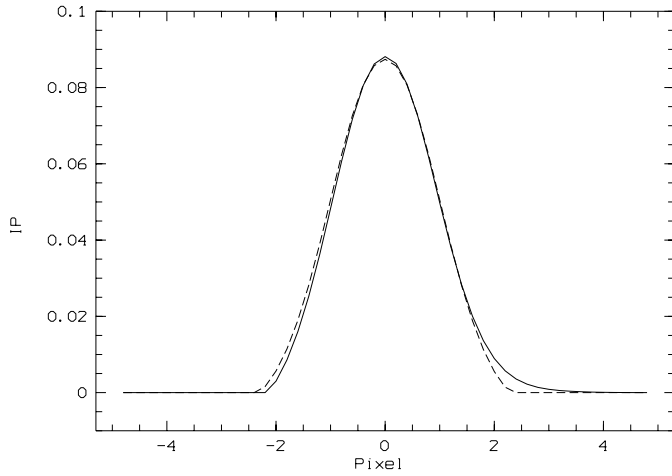


**Fig. 4.** Variation of the CES instrumental profile in the course of one night. 7 domeflat  $I_2$ -spectra were taken at the beginning and 4 at the end of the night. IPs were reconstructed for all domeflatfield spectra and compared with one another. The plot shows the greatest difference we found for two IPs reconstructed for the wavelength region of 538.8 nm from the beginning (solid line) and from the end of the night (dashed line).

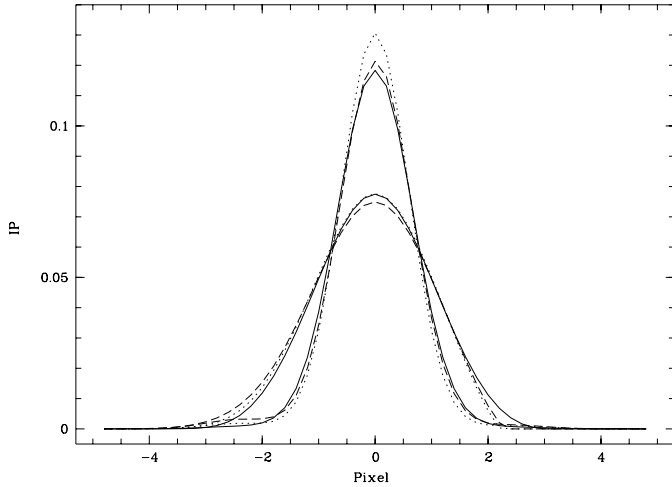


**Fig. 5.** Extreme CES instrumental profile variation due to setup changes of the spectrograph. Reconstructed IPs are shown for the nights of March 2nd 1994 (sharp IPs) and January 14th 1995 (broad IPs). The variation is apparent in the results of both the flatfield lamp (solid lines) and the B-star  $I_2$ -spectra taken in those nights (dotted lines). Furthermore, consistent IP shapes are reconstructed by step 3 modeling (see Sect. 3.3) of two star & iodine spectra of HR 6998 (1994) and  $\tau$  Cet (1995), taken in the same nights (dashed lines).

which constitutes the matrix equation:

$$\vec{g} = \Phi \vec{f} \quad (8)$$

Since the matrix  $\Phi$  can be calculated from the vector  $\vec{\phi}$  obtained in step 1, MEM can be used to solve Eq. (8) for the vector  $\vec{f}$  to recover an approximation to the intrinsic spectrum.

Before applying this method to a real star spectrum we tested our MEM deconvolution approach on simulated data. Fig. 6 illustrates one test case, where we simulated two half-blended

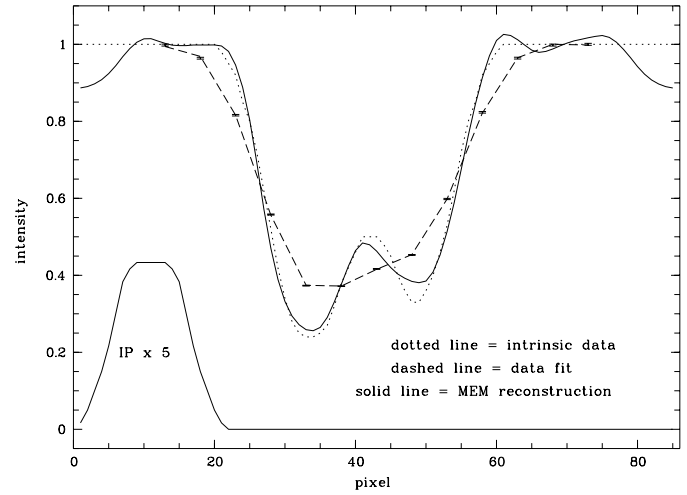


**Fig. 6.** Simulated test case for the Maximum Entropy deconvolution. Two half-blended absorption lines (dotted line) are convolved with an assumed IP (shown in the lower left corner, five times magnified in  $y$  for display purposes) to simulate the observation (dots with errorbars). The solid line represents the MEM reconstruction of the intrinsic spectrum  $f$  and the corresponding fit to the observation (with  $\chi^2 = N$ ,  $N$  number of data points) is shown as a dashed line ( $= f \otimes \text{IP}$ ). Deviations of the MEM reconstruction from the intrinsic spectrum seen at the beginning and at the end of the chunk are edge effects, which are avoided during the deconvolution of real spectra by using suitably overlapping spectral chunks.

absorption lines which are not resolved in the actual observation. The simulated observation ( $\vec{g}$ ) is created by convolving the (known) intrinsic spectrum (shown in Fig. 6 as a dotted line) with an assumed IP. This IP is taken to compute the matrix  $\Phi$  which together with the observation  $\vec{g}$  serves as input for MEM. The  $\chi^2$ -statistic is used for the “goodness-of-fit” check. MEM iterates until  $\chi^2 = N$  ( $N$  is the number of data points  $g(i)$ ) is reached. Clearly, the MEM deconvolution successfully recovers the structure of the intrinsic spectrum. This simulation is of course limited by the fact that the IP taken for the deconvolution is exactly known (which is never the case for real data) and that the error (noise) of the simulated observation is very small.

One problem of most deconvolution methods is the conservation of flux. Although this aspect is not critical for RV measurements, where the position and symmetry of the spectral line contains the important information, we performed a series of numerical simulations to examine this subject. We took synthetic Gaussian-shaped absorption lines with three different line depths (90, 65 and 30% of the continuum level) and  $S/N$ -ratios of 100, 200, and 300 and compared the areas before and after deconvolution. For the shallow line and for a  $S/N$ -ratio of 100 the flux was conserved by 76%, for  $S/N$ -ratio 200 by 92% and for  $S/N=300$  by 96%. The corresponding results for the medium line case are 94%, 99%, and 100%, while for the strong line we found 98%, 99%, and 99%. These results demonstrate clearly the importance of a higher  $S/N$ -ratio of the pure star spectra

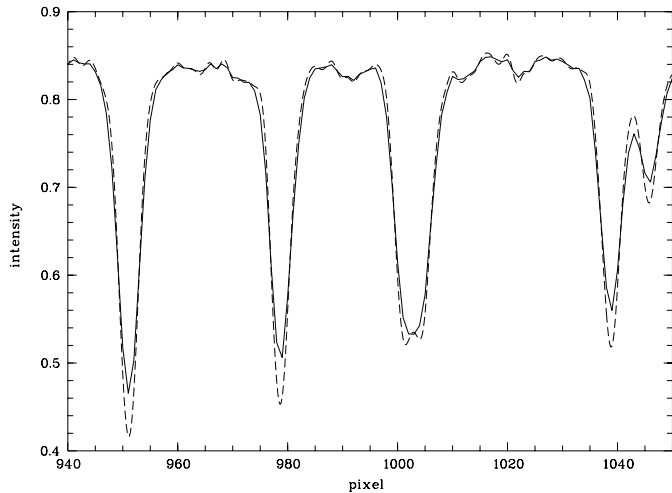


**Fig. 7.** One section of a CES spectrum of  $\delta$  Eri (solid line) compared to the deconvolved spectrum (dashed line) obtained by the Maximum Entropy Method and reconstructed IPs from an  $I_2$ -spectrum of the same night. The wavelength region from 538.62 to 538.85 nm is displayed.

selected to serve as template spectra for the modeling (the  $S/N$ -ratios we use always exceed 100).

For the deconvolution we reconstruct the corresponding IPs with iodine spectra taken on the same night as the stellar spectrum was obtained. We observe rapidly rotating B-stars, lacking any spectral features in the wavelength regime around 538.9 nm, with the  $I_2$ -cell located in the light path. In this way the light path resembles closely the configuration of stellar observations without the cell. However, if no B-star  $I_2$ -spectrum is available we use domeflat  $I_2$ -spectra for the IP reconstruction. Fig. 7 demonstrates one result of the MEM deconvolution applied to a spectrum of the K0IV star  $\delta$  Eri (HR 1136).

After the deconvolution a cubic spline interpolation is applied and the template is set up in exactly the same way as the FTS-based template of the iodine spectrum in step 1 (see also Sect. 3.1). The wavelength calibration of the template is performed using an 6th-order dispersion polynomial which is obtained by measuring the positions of ThAr lines in calibration exposures taken in the same night.

### 3.3. Step 3: full modeling of the combined star and iodine spectrum

In this final step the combined star & iodine spectrum is modeled to obtain radial velocities. This step is in principle equivalent to step 1 with the extension that now the stellar spectrum is also present in the observation. When the starlight passes through the  $I_2$ -cell a simple multiplication of the stellar with the iodine spectrum takes place. Hence in Eq. (1)  $f(x')$  is the product of the intrinsic star spectrum and the intrinsic iodine spectrum. The  $I_2$ -FTS and the deconvolved stellar spectrum from step 2 serve as model templates to synthesize the observation. With the presence of a second template, additional parameters have to be included in the optimization algorithm. Again the spectrum is subdivided into smaller spectral chunks and the multi-

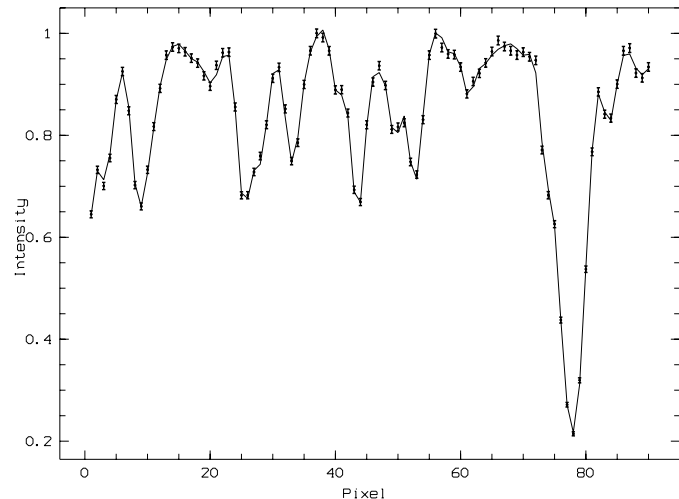


**Fig. 8.** Example of the modeling result (solid line) for a 90 pixel chunk of a  $\delta$  Eri spectrum (dots and errorbars). One deep stellar absorption line is clearly visible to the right, while most of the shallower lines are iodine reference lines.

parameter optimization is applied to achieve a best-fit model for each chunk (see Fig. 8). Moreover, since each chunk is modeled independently it can be treated in the overall RV statistics of the spectrum as one independent RV measurement. As in step 1 the shape and asymmetry of the spectrograph IP is reconstructed during this process. The formally best-fit (with lowest  $\chi^2$ -values) for star & iodine spectra is usually achieved by employing the Multi-Gaussian plus MEM correction IP mode. For a typical spectrum with a mean  $S/N$ -ratio of 120 we usually get reduced  $\chi^2$ -values of 1.4–1.5 for the 90-pixel chunks (degrees of freedom = 75). The IP reconstructions in step 3 are also consistent with the results obtained in step 1 using pure  $I_2$ -spectra (see the comparison in Fig. 5). The long-term character of the CES planet search program also allows the monitoring of the IP over a long time period. Fig. 9 illustrates the differences in reconstructed IP shapes over the time span from November 1992 to October 1997.

After having attained the best-fit model, the radial velocity is computed for each chunk of the spectrum from the Doppler shift  $\delta\lambda$  between the  $I_2$  and the star model. Using the wavelength zero-point parameters and the dispersion parameters a corresponding position in wavelength is computed for every oversampling pixel of both models (the iodine and the star model respectively). From this information the Doppler shift between iodine and stellar lines is calculated and transformed into radial velocity. The actual RV result and its error for the whole spectrum is obtained by running a statistics over the RV results of all chunks (see Fig. 10). Typically 20 to 22 spectral chunks are analysed per spectrum and chunks with outlying RV results (further off than  $3\sigma$  from the mean value of the spectrum) are rejected. As the error of the final RV value we take the error of the mean value ( $= \text{RMS}/\sqrt{N}$ , with  $N$  the number of unrejected chunks). Finally the velocity correction to the solar system barycenter is applied; this correction is calculated by use of the JPL ephemeris

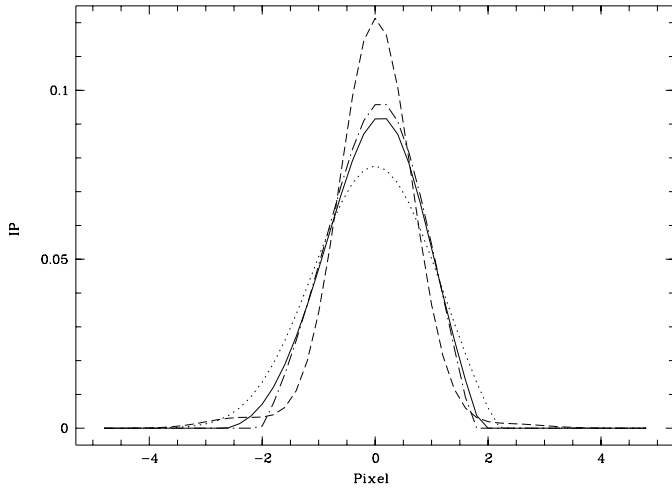


**Fig. 9.** CES instrumental profile monitoring over five years. IP modeling results are displayed for four different stellar & iodine spectra taken on the nights of November 3rd 1992 (solid line), March 2nd 1994 (dashed line), January 14th 1995 (dotted line) and October 10th 1997 (dots & dashed line). IPs were reconstructed for the wavelength region of 538.7 nm using spectra of  $\tau$  Cet (1992 & 1995) and HR 6998 (1994 & 1997).

DE200 (e.g. Standish 1990). For the calculation of this velocity correction we also take proper motion effects into account.

#### 4. RV precision tests

For precision testing we chose three stars with known RV pattern, the RV-constant star  $\tau$  Cet and two stars with known extrasolar planets and well determined orbits, 51 Peg and 70 Vir (see also Endl et al. 2000). Furthermore, we examine the long-term RV behavior of  $\alpha$  Men and GJ 570A, two typical stars from the CES planet search survey.

##### 4.1. $\tau$ Cet

$\tau$  Cet (HR 509, HD 10700), a G8V star with  $V = 3.5$  has earlier been identified as one of the most stable stars in radial velocity (Campbell et al. 1988; Walker et al. 1995) and was measured by the Lick Planet Search survey (Butler et al. 1996) and by the AAT Doppler survey (Butler, private communication) as constant within their measurement errors of about  $5 \text{ ms}^{-1}$ . In the time interval from November 1992 to January 1998 the CES planet search program collected a total of 116 spectra of  $\tau$  Cet, ranging in  $S/N$ -ratio from 71 to 275. Analysis with our modeling technique yielded a total scatter of  $11.3 \text{ ms}^{-1}$  over the time span of five and a half years (see upper panel of Fig. 11). The average internal measurement error is  $14.1 \text{ ms}^{-1}$  with a maximum value of  $24.4 \text{ ms}^{-1}$  for the spectrum with the lowest  $S/N$ -ratio and  $6.9 \text{ ms}^{-1}$  as the best value. The importance of the reconstruction of IP asymmetries is also demonstrated in Fig. 11, where the lower panel shows results of an analysis of the same data, using only the Single-Gaussian IP mode during the modeling. Still, some IP modeling was performed, with the width of the IP being optimized, but no asymmetries in the IP

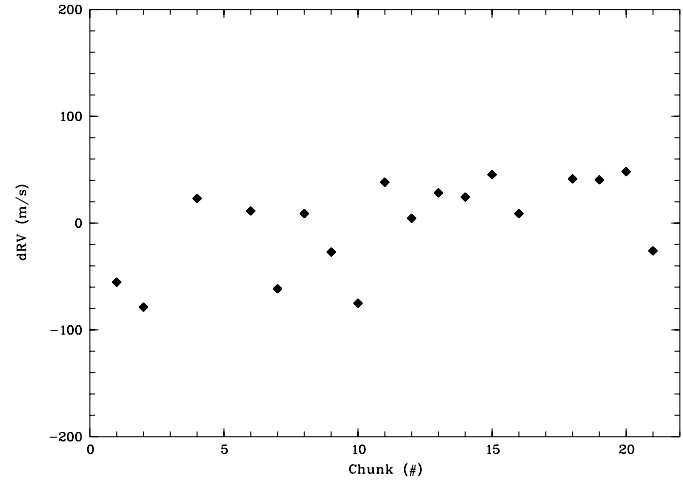


**Fig. 10.** Distribution of individual relative radial velocities determined for each chunk of a CES spectrum of  $\tau$  Cet. Chunk #3, #5 and #17 are further off than  $3\sigma$  from the mean and hence rejected as outliers. The remaining 18 chunks have an RMS of  $43.03 \text{ ms}^{-1}$  corresponding to an internal error of the mean RV of  $10.14 \text{ ms}^{-1}$ . The varying number and strength of the stellar absorption lines along the spectrum introduces a non-Gaussian distribution of errors. Typically, 1–2 chunks are rejected for CES spectra, showing here a worse case where even 3 chunks were found to be outliers.

shape were taken into account. The previous result of  $11.3 \text{ ms}^{-1}$  with asymmetric IP reconstruction is more than a factor of 3 better than the  $36.2 \text{ ms}^{-1}$  obtained with only symmetric IP modeling. Fig. 12 demonstrates the short-term RV precision of the CES by comparing 10 individual measurements of  $\tau$  Cet taken within one hour during one night. The actual long-term precision of  $11.3 \text{ ms}^{-1}$  (and even more the short-term precision) is higher than the average internal error would suggest. This can be explained by the fact that the differential character of the RV measurements is not very susceptible to residual systematic patterns within the internal RV distribution of the spectra (this effect is even more obvious in our test results for 51 Peg).

##### 4.2. 51 Peg

51 Peg (HR 8729, HD 217014) was the first solar-type star (spectral type G5V,  $V = 5.45$ ) discovered with a planetary companion (Mayor & Queloz 1995). The well established orbital solution (Marcy et al. 1997) of this short period planet ( $P = 4.23$  days) allowed us to perform another precision test. 51 Peg was observed on seven different nights during the CES planet search survey. Fig. 13 shows our analysis results, with a total RMS of  $14.4 \text{ ms}^{-1}$  around the known orbit. The error bars represent the internal errors and are larger than the actually achieved precision as determined from the fit to the orbit, again demonstrating that the differential measurements are in fact more precise than the internal errors suggest (a systematic RV distribution present in all spectra increases the internal RMS but does not affect the relative measurements to the same extent).

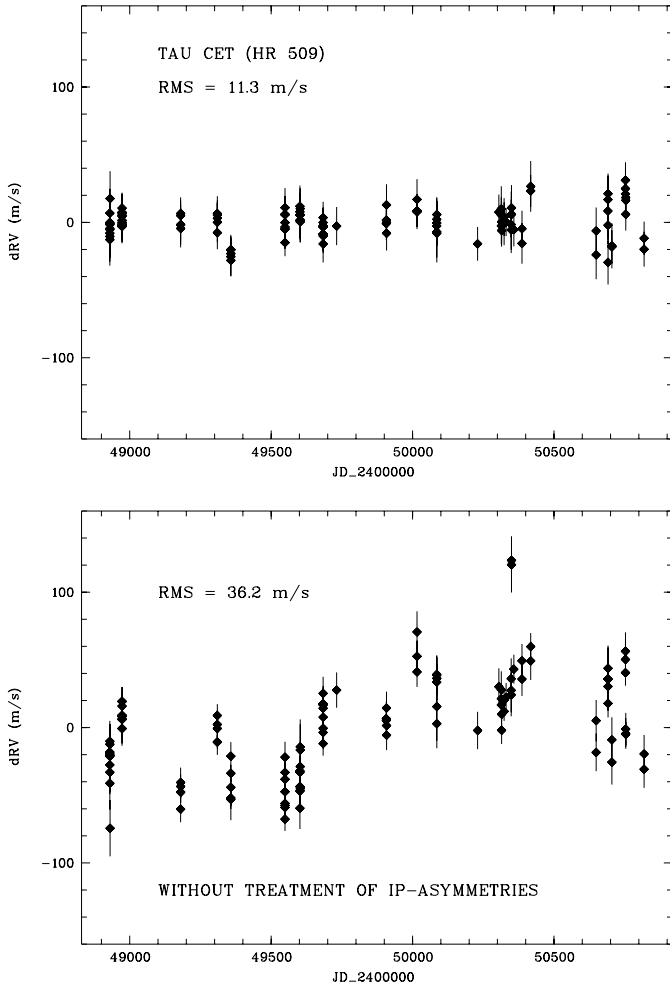


**Fig. 11.** Differential radial velocities of the RV-constant star  $\tau$  Cet (HR 509). Five and a half years of data collected with the CES spectrograph and the 1.4m CAT telescope are shown. The total scatter of  $11.3 \text{ ms}^{-1}$  (upper panel) represents the long-term precision for  $\tau$  Cet achieved with the  $I_2$ -cell and our data modeling technique for the CES spectrograph in the Long Camera configuration. The lower panel shows the same  $\tau$  Cet data set analysed without taking IP asymmetries into account. The resulting long-term scatter in RV is more than a factor of 3 higher than in the previous case, demonstrating the importance of the modeling of IP-asymmetries.

#### 4.3. 70 Vir

70 Vir (HR 5072, HD 117176) was used for the final precision check. The G4V star 70 Vir ( $V = 4.98$ ) is orbited by an extra-solar planet with a projected minimum mass of  $7.1 M_{\text{Jup}}$  in a 116-day eccentric ( $e=0.38$ ) orbit (Marcy & Butler 1996). As in the case of 51 Peg seven observations were obtained with the CES. Fig. 14 summarizes the result of the modeling of these spectra. Again orbital residuals are smaller than  $15 \text{ ms}^{-1}$ .

#### 4.4. $\alpha$ Men

The example of  $\alpha$  Men (HR 2261, HD 43834), which can be taken as a typical star in the CES planet search survey sample

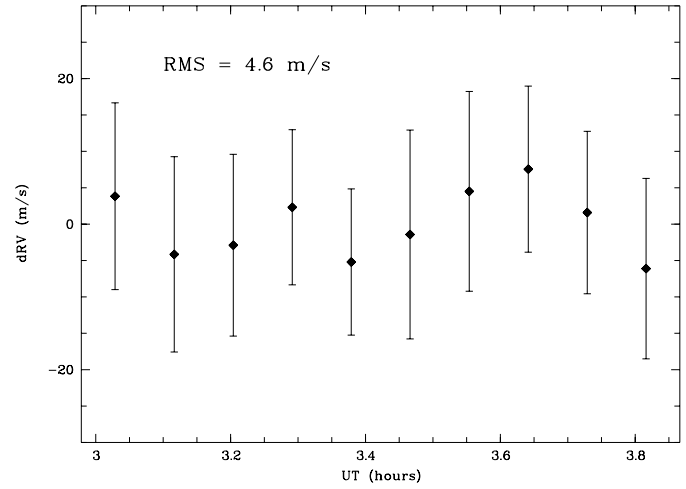


**Fig. 12.** RV short-term precision of the CES. On the night of December 16th, 1992 ten consecutive spectra of  $\tau$  Cet were taken over a time span of 50 minutes. All spectra have the same exposure time of 4 minutes and similar S/N-ratios. The RV results after the analysis exhibit a small scatter of  $4.6 \text{ ms}^{-1}$ , demonstrating the CES short-term RV precision for a bright, chromospherically quiet G8V star. By applying the F-test we can exclude with a confidence of 95% (99%) that the true measurement error is higher than  $7.6$  ( $9.5$ )  $\text{ms}^{-1}$ .

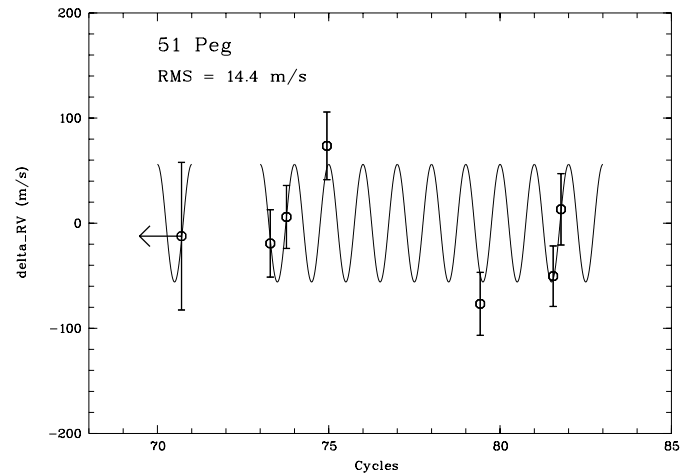


**Fig. 13.** Differential radial velocities of 51 Peg determined from seven observations with the CAT telescope and the CES spectrograph. The solid line represents the known orbital solution (Marcy et al. 1997) with the adjusted velocity zero-point. Orbital residuals were found to be  $14.4 \text{ ms}^{-1}$ . Note that for display purposes the first measurement is shifted by 70 orbital cycles (indicated by the arrow).

(G6V star with  $V = 5.1$ ), verifies the long-term precision found in the  $\tau$  Cet data. The analysis results of 41  $\alpha$  Men spectra exhibit no RV variation and a total RMS of  $9.8 \text{ ms}^{-1}$  over the time period from March 1993 to April 1998 (see Fig. 15). Within the given CES precision we conclude that  $\alpha$  Men is another long-term RV-constant star.

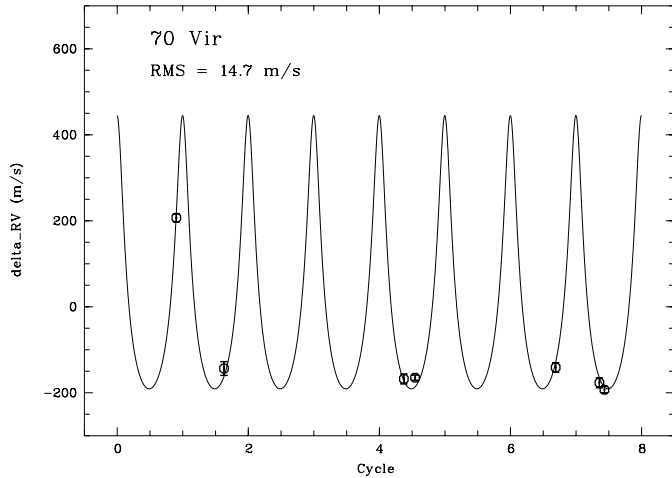


**Fig. 14.** Test results for 70 Vir showing differential radial velocities over eight orbital cycles. Seven observations were obtained with the CES spectrograph over two years. After the velocity zero-point has been adjusted the residuals from the known orbit (Marcy & Butler 1996) are smaller than  $15 \text{ ms}^{-1}$ .

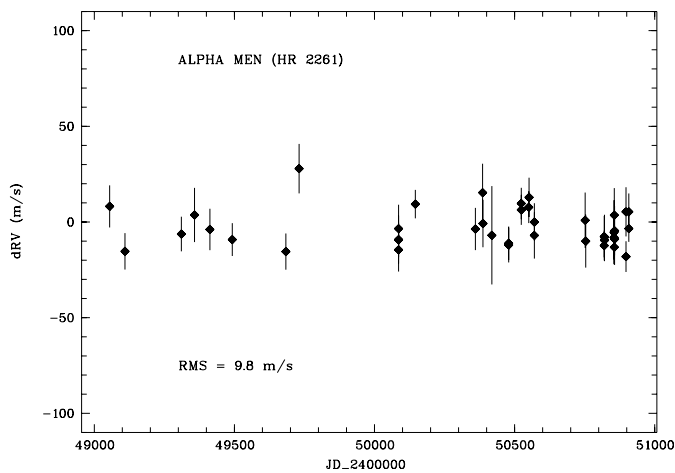


**Fig. 15.** Five years of radial velocities of the G6V star  $\alpha$  Men (HR 2261, HD 43834,  $V = 5.1$ ). The total RMS of  $9.8 \text{ ms}^{-1}$  verifies the long-term precision we found for  $\tau$  Cet.

#### 4.5. GJ 570A

GJ 570A (HR 5568, HD 131977,  $V = 5.74$ ), a nearby K4V ( $d = 5.91 \text{ pc}$ ) star was included in the CES sample as a Hipparcos astrometric candidate for having a close brown dwarf companion (Bernstein, 1997). The best astrometric orbital solution given by Bernstein suggests an  $0.06 \pm 0.02 M_{\odot}$  companion in a nearly edge-on orbit with a period of 33 days. Such a companion would cause an RV variation of the order of a few  $\text{km s}^{-1}$  and would be easily detectable. Preliminary results from CES data obtained over a time span of almost one year did not reveal such a huge RV amplitude (Kürster et al. 1999), only a small possible variation ( $K \approx 50 \text{ ms}^{-1}$ ) was indicated by an analysis of the CES spectra with a method, which does not include higher resolved model templates and IP reconstruction. After re-analysing all 40 CES Long Camera spectra of GJ 570A

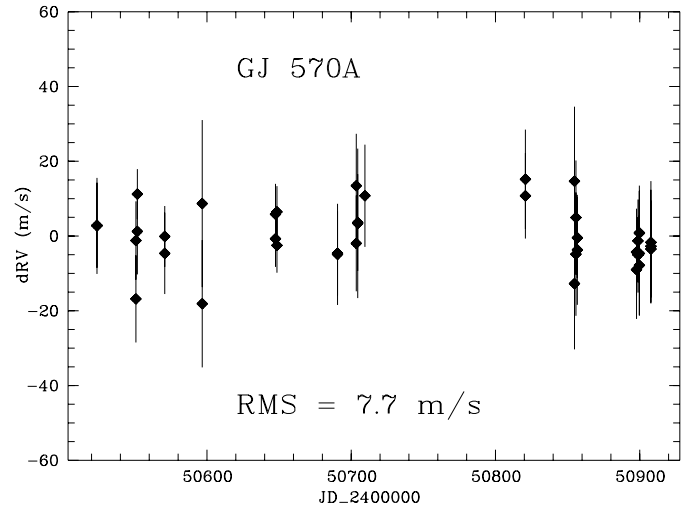


**Fig. 16.** 1 year of radial velocities of GJ 570A (HR 5568, HD 131977, HIP 73184). The long-term RV scatter of  $7.7 \text{ ms}^{-1}$  shows our best case in achieved RV precision for CES Long Camera data.

with our new technique we found the RV scatter to be reduced to  $12.4 \text{ ms}^{-1}$ . Moreover, we have obtained a high  $S/N$  pure star spectrum using the 3.6m telescope and the CES in the Very Long Camera (VLC) & CCD #59 configuration, which yields a higher resolving power of  $R \approx 220,000$ . Although by using this spectrum as the stellar template, the working spectral bandwidth is even reduced to only  $3.59 \text{ nm}$  (the VLC & CCD #59 bandpass), the RV scatter is lowered to  $7.7 \text{ ms}^{-1}$  (see Fig. 16). This result is also confirmed by the Lick Planet Search, where GJ 570A is found to be constant since 1994 with an overall scatter of  $11.3 \text{ ms}^{-1}$  (Cumming et al. 1999). It is clear that a close-by brown dwarf companion (and even a giant planet) can be excluded from the RV data, making GJ 570A even our “best case”, with the lowest long-term RV scatter in our sample so far.

## 5. Outlook

The astrophysical application of the modeling technique is of course not limited to the search for substellar companions. Other applications could include the examination of the amplitudes and periods of stellar pulsation modes or the dependence of RV patterns on stellar activity levels. A new project will attempt to disentangle activity related RV shifts (e.g. Hatzes 1999) from the gravitationally induced reflex motion in order to search for planets around young stars (Els et al. 1999).

The CES planet search program is currently continuing with the 3.6m telescope on La Silla. After the decommissioning of the CAT telescope in summer 1998, the CES has been connected to the 3.6m telescope via a fibre-link. Since we have emphasized the flexibility of our method, we have been successful in modeling spectra taken with the Very Long Camera now installed at the CES, which raised the resolving power to  $R = 220,000$ . Also, we were able to analyse data from different spectrographs and telescopes. We tested our method successfully on pure  $I_2$ -spectra obtained with the FEROS spectrograph mounted at the

ESO 1.5m telescope (using the CES I<sub>2</sub>-cell) as well as on a laboratory I<sub>2</sub>-spectrum of the I<sub>2</sub>-cell at the UVES instrument (now mounted at the ESO VLT/UT2 8.2m telescope). Furthermore, application to data from the McDonald 2.7m+Coudé and Keck HIRES was also performed successfully (Hatzes, private communication).

With the empirical values of the internal and actually achieved long-term precision for CES data of  $\tau$  Cet we can perform a crude extrapolation of the precision we would reach by applying our modeling technique to spectra covering a much larger wavelength range, typically obtained by multi-order cross-dispersed Echelle spectrometers. Actually the useful wavelength regime is limited by the fact that the I<sub>2</sub>-cell provides a dense reference spectrum only over a certain part of the visible spectrum. The I<sub>2</sub>-cell in use at the CES has a working bandwidth of about 100 nm. From this we extrapolate a total quantity of 500 chunks, from which we conservatively reject 20% as outliers, ending up with 400 useful chunks. Now with an average RMS of 60 ms<sup>-1</sup> for the 4.85 nm spectrum and the assumption that systematic effects would increase the RMS by 50% over the longer 100 nm spectrum, we would attain an internal error of 4.5 ms<sup>-1</sup> and a corresponding long-term precision of about 3.6 ms<sup>-1</sup> (assuming again that it is about 20% better than the average internal error). Applying our method to cross-dispersed spectra calibrated with an I<sub>2</sub>-spectrum covering even a larger spectral range would improve the measurement precision even further. The I<sub>2</sub>-cell currently installed at the UVES spectrograph at the ESO VLT/UT2 8.2m telescope on Paranal delivers useful reference lines over a range of 150 nm. The UVES instrument has a higher resolving power ( $R = 120,000$ ) than the CES and an RMS of 100 ms<sup>-1</sup> along a UVES spectrum would yield an internal error of 4 ms<sup>-1</sup> and a long-term precision of 3.2 ms<sup>-1</sup>, while a smaller RMS of 50 ms<sup>-1</sup> would raise the internal measurement precision to 2 ms<sup>-1</sup> and reduce the long-term scatter of  $\tau$  Cet to 1.6 ms<sup>-1</sup>, a factor of 7 better than the CES.

## 6. Summary

1. We describe the modeling technique in use for the analysis of the CES planet search data.
2. The modeling process includes various different ways to reconstruct the spectrograph instrumental profile (IP).
3. We developed a Maximum Entropy Method approach to deconvolve pure star spectra to obtain higher resolution templates.
4. The final modeling step computes high precision stellar radial velocities by synthesizing the observed iodine & star spectrum with higher resolved model templates.
5. We show IP variations of the CES on short and long time scales, demonstrating the importance of IP modeling for CES data from different observing runs.
6. For the short CES spectra (4.85 nm) we achieve an RV measurement precision of 8–15 ms<sup>-1</sup>. In the cases of  $\tau$  Cet and  $\alpha$  Men a long-term precision of 11.3 & 9.8 ms<sup>-1</sup> over five and a half years was attained.
7. For GJ 570A we reach an RV precision of 7.7 ms<sup>-1</sup> for the time span of one year, excluding the presence of a short period brown dwarf companion.

*Acknowledgements.* We thank the ESO OPC for generous allocation of observing time. We would like to thank Artie Hatzes, Konrad Dennerl and Stefan Döbereiner for doing part of the observations of the program. Furthermore, we thank William Cochran and Artie Hatzes for important discussions about this work. We are grateful to A. Hatzes and G. Marcy who obtained the FTS scan of our iodine cell at Kitt Peak. ME and MK also thank M. Vannier for his contribution at the beginning of this work. A fast algorithmic approach to Maximum Entropy solutions was outlined to us by M. Warmuth. We thank the anonymous referee for his suggestions for this article. ME acknowledges support by the Austrian Fond zur Förderung der wissenschaftlichen Forschung Nr. S7302.

## References

- Bernstein H.-H., 1997, In: Proceedings of the ESA Symposium ‘Hipparcos - Venice 97’, 13–16 May, Venice, Italy, ESA AP-402 (July 1997), p. 705
- Butler R.P., Marcy G.W., Williams E., et al., S.S., 1996, PASP 108, 500
- Campbell B., Walker G.A.H., Yang S., 1988, ApJ 331, 902
- Cochran W.D., Hatzes A.P., Butler R.P., Marcy G.W., 1997, ApJ 483, 457
- Cumming A., Marcy G.W., Butler R.P., 1999, ApJ 526, 890
- Els S., Kürster M., Endl M., 1999, In: AG Abstract Series vol.15, P18, 96
- Endl M., Kürster M., Els S., 2000, In: Griffith C., Marley M. (eds.) From Giant Planets to Cool Stars. ASP Conf. Ser., in press
- Fischer D.A., Marcy G.W., Butler R.P., Vogt S.S., Apps K., 1999, PASP 111, 50
- Hatzes A.P., Kürster M., Cochran W.D., Dennerl K., Döbereiner S., 1996, J. Geophys. Research (Planets) 101, 9285
- Hatzes A.P., 1999, In: Hearnshaw J.B., Scarfe C.D. (eds.) Precise Stellar Radial Velocities. Proc. IAU Coll. 170, ASP Conf. Ser. 185, p. 259
- Kivinen J., Warmuth M.K., 1997, Journal of Information and Computation, Vol. 132, No. 1, p. 1
- Kürster M., Hatzes A.P., Cochran W.D., et al., Döbereiner S., 1994, The ESO Messenger 76, 51
- Kürster M., Hatzes A.P., Cochran W.D., et al., 1999, In: Hearnshaw J.B., Scarfe C.D. (eds.) Precise Stellar Radial Velocities. Proc. IAU Coll.170, ASP Conf. Ser. 185, p. 154
- Kürster M., Endl M., Els S., et al., Döbereiner S., Dennerl K., 2000, A&A 353, L33
- Marcy G.W., Butler R.P., 1996, ApJ 464, L147
- Marcy G.W., Butler R.P., Williams E., et al., 1997, ApJ 481, 926
- Mayor M., Queloz D., 1995, Nat 378, 355
- Noyes R.W., Jha S., Korzennik S.G., et al., 1997, ApJ 483, L111
- Press W.H., Teukolsky S.A., Vetterling W.T., Flannery B.P., 1992, In: Numerical Recipes: The Art of Scientific Computing. 2nd ed., Cambridge University Press, New York
- Standish E.M., 1990, A&A 233, 252
- Valenti J.A., Butler R.P., Marcy G.W., 1995, PASP 107, 966
- Walker G.A.H., Walker A.R., Irwin A.W., et al., 1995, Icarus 116, 359